



HAL
open science

Identification of a peripheral blood gene signature predicting aortic valve calcification

Donal Macgrogan, Beatriz Martínez-Poveda, Jean-Pierre Desvignes, Leticia Fernandez-Friera, Manuel José Gomez, Eduardo Gil Vilariño, Sergio Callejas Alejano, Pablo García-Pavía, Jorge Solis, Joaquín Lucena, et al.

► **To cite this version:**

Donal Macgrogan, Beatriz Martínez-Poveda, Jean-Pierre Desvignes, Leticia Fernandez-Friera, Manuel José Gomez, et al.. Identification of a peripheral blood gene signature predicting aortic valve calcification. *Physiological Genomics*, 2020, 52 (12), pp.563-574. 10.1152/physiolgenomics.00034.2020 . hal-02965646

HAL Id: hal-02965646

<https://amu.hal.science/hal-02965646>

Submitted on 28 Apr 2021

HAL is a multi-disciplinary open access archive for the deposit and dissemination of scientific research documents, whether they are published or not. The documents may come from teaching and research institutions in France or abroad, or from public or private research centers.

L'archive ouverte pluridisciplinaire **HAL**, est destinée au dépôt et à la diffusion de documents scientifiques de niveau recherche, publiés ou non, émanant des établissements d'enseignement et de recherche français ou étrangers, des laboratoires publics ou privés.

1 **MS PG-00034-2020 revised: Identification of a peripheral blood gene signature predicting**
2 **aortic valve calcification**

3 Running title: A gene signature predicting aortic valve calcification

4
5 *Supplemental Material and Suppl. Tables* available at:

6
7 [URL: https://figshare.com/s/d9a68e0d6faa67e4c6c3](https://figshare.com/s/d9a68e0d6faa67e4c6c3) and <https://figshare.com/s/4357d56025cb3380a0df>

8
9 [DOI: 10.6084/m9.figshare.12086712](https://doi.org/10.6084/m9.figshare.12086712) and [10.6084/m9.figshare.12086724](https://doi.org/10.6084/m9.figshare.12086724)

10
11
12 Donal MacGrogan^{1,2,*}, Beatriz Martínez Poveda^{1,2}, Jean-Pierre Desvignes³, Leticia Fernandez-Friera^{2,4,5},
13 Manuel José Gomez⁶, Eduardo Gil Vilariño⁷, Sergio Callejas Alejano⁷, Pablo Garcia-Pavia^{2,8,9}, Jorge
14 Solis¹⁰, Joaquín Lucena¹¹, David Salgado³, Gwenaelle Collod-Bérout³, Emilie Faure³, Alexis Théron¹²,
15 Julia Torrents¹³, Jean-François Avierinos^{3,12}, Lorena Montes¹⁴, Ana Dopazo⁷, Valentín Fuster^{15,16}, Borja
16 Ibañez^{2,17}, Fátima Sánchez-Cabo⁶, Stephane Zaffran³ & José Luis de la Pompa^{1,2,*}

17
18 ¹ Intercellular Signaling in Cardiovascular Development & Disease laboratory, Centro Nacional de
19 Investigaciones Cardiovasculares Carlos III (CNIC), Melchor Fernández Almagro 3, 28029 Madrid,
20 SPAIN

21 ² Ciber de Enfermedades Cardiovasculares, Instituto de Salud Carlos III, Melchor Fernández Almagro 3,
22 28029 Madrid, SPAIN

23 ³ Aix Marseille University, MMG, INSERM U1251, Marseille, FRANCE

24 ⁴ Translational Laboratory for Cardiovascular Imaging and Therapy, CNIC, SPAIN

25 ⁵ HM Hospitales-Centro Integral de Enfermedades Cardiovasculares, Madrid, SPAIN

26 ⁶ Bioinformatics Unit, CNIC, SPAIN

27 ⁷ Genomics Unit, CNIC, SPAIN

28 ⁸ Departamento de Cardiología, Hospital Universitario Puerta de Hierro, Madrid, SPAIN

29 ⁹ Universidad Francisco de Vitoria, Pozuelo de Alarcón, Madrid, SPAIN

30 ¹⁰ Departamento of Cardiología, Hospital Universitario Doce de Octubre, Madrid, SPAIN

31 ¹¹ Servicio de Patología Forense, Instituto de Medicina Legal y Ciencias Forenses,
32 Sevilla, SPAIN

33 ¹² Service de Cardiologie, Hôpital de la Timone, 13005, Marseille, FRANCE

34 ¹³ Service d'anatomie et Cytologie Pathologiques, Hôpital de la Timone, 13005, Marseille, FRANCE

35 ¹⁴ Hospital Clínico San Carlos, Madrid, SPAIN

36 ¹⁵ Cardiovascular Imaging and Population Studies Laboratory, CNIC, SPAIN

37 ¹⁶ Cardiology Department, Icahn School of Medicine at Mount Sinai, New York, New York, USA

38 ¹⁷ IIS-Fundación Jiménez Díaz Hospital Universitario, Madrid, SPAIN

39 * Corresponding authors

40 **Correspondence:**

41 José Luis de la Pompa

42 Intercellular Signaling in Cardiovascular Development & Disease laboratory

43 Centro Nacional de Investigaciones Cardiovasculares Carlos III (CNIC)

44 Melchor Fernández Almagro 3, 28029 Madrid, SPAIN.

45 Tel: +34 91 4531200

46 Email: jlpompa@cnic.es

47 **ABSTRACT**

48

49 Calcific aortic valve disease (CAVD) is a significant cause of illness and death worldwide.
50 Identification of early predictive markers could help optimize patient management. RNA-
51 sequencing was carried out on human fetal aortic valves at gestational weeks 9, 13, and 22, and
52 on a case-control study with adult non-calcified and calcified bicuspid and tricuspid aortic
53 valves. In dimension reduction and clustering analyses, diseased valves tended to cluster with
54 fetal valves at week 9 rather than normal adult valves, suggesting that part of the disease
55 program might be due to re-iterated developmental processes. The analysis of groups of co-
56 regulated genes revealed predominant immune-metabolic signatures, including innate and
57 adaptive immune responses involving lymphocyte T cell metabolic adaptation. Cytokine and
58 chemokine signaling, cell migration, and proliferation were all increased in CAVD, whereas
59 oxidative phosphorylation and protein translation were decreased. Discrete immune-metabolic
60 gene signatures were present at fetal stages and increased in adult controls, suggesting that these
61 processes intensify throughout life and heighten in disease. Cellular stress-response and
62 neurodegeneration gene signatures were aberrantly expressed in CAVD, pointing to a
63 mechanistic link between chronic inflammation and biological ageing. Comparison of the valve
64 RNA-sequencing dataset with a case-control study of whole blood transcriptomes from
65 asymptomatic individuals with early aortic valve calcification identified a highly predictive gene
66 signature of CAVD and of moderate aortic valve calcification in overtly healthy individuals.
67 These data deepen and broaden our understanding of the molecular basis of CAVD and identify
68 a peripheral blood gene signature for the early detection of aortic valve calcification.

69

70 **Keywords**

71 Human fetal valve; CAVD; inflammation; peripheral blood biomarker; gene signature

72 **INTRODUCTION**

73 Calcific aortic valve disease (CAVD) is caused by calcium build-up of the aortic valve leaflet
74 and may be associated with hemodynamic obstruction, leading to different degrees of aortic
75 stenosis (AS). Untreated severe AS leads to heart failure, with valve replacement remaining the
76 only available treatment. Severe AS is preceded by aortic sclerosis, a subclinical form of CAVD
77 that develops over many years without hemodynamic consequence (6). The prevalence of aortic
78 valve disorders increases with age, with 25% of individuals >65 years with aortic sclerosis
79 progressing to AS at a rate of 2% per year (4). Other than age, the principal CAVD risk factor for
80 AS is a congenitally malformed bicuspid aortic valve (BAV), which is present in 0.5-2% of the
81 general population (31). Patients with AS and a BAV are a decade younger at diagnosis than
82 those with normal tricuspid aortic valve (TAV) morphology (2). Premature leaflet thickening and
83 calcification in BAV patients may be caused by abnormal shear stress hemodynamics.

84 CAVD shares mechanistic features with atherosclerosis (6). The current accepted model
85 implicates initial lipid oxidation, inflammatory infiltration by T-lymphocytes and macrophages,
86 cytokine and pro-fibrotic signaling, and altered extracellular matrix (ECM) secretion, leading to
87 ectopic bone formation and tissue mineralization (11, 22). The factors predicting transition from
88 the “at risk” status to aortic sclerosis and subsequently to severe AS, are not known (25).
89 Transcriptional profiling of CAVD has helped to identify hundreds of genes differentially
90 expressed between calcified and normal valves (8). Multi-omics approaches combining
91 transcriptomics and proteomics have provided a high-resolution expression atlas and established
92 potential drivers of disease progression (30).

93 Despite this progress, thus far no medical therapy has been proven to be effective in
94 preventing progression to severe disease, with randomized clinical trials demonstrating the lack
95 of effect of statins on disease progression (36). It has been suggested that statin treatment would
96 have to begin at an earlier disease stage to have a beneficial effect. Current imaging modalities,
97 especially echocardiography, remain the gold standard for diagnosis of valve disease but are

98 mainly performed when symptoms appear. Non-contrast computed tomography may have
99 significant predictive value in both asymptomatic and symptomatic patients, but remains a
100 source of radiation exposure and may not be available in centers with limited resources.
101 Biomarkers may complement imaging modalities to detect early changes, especially early
102 calcification. The ideal biomarker would predict disease as well as improve prognosis,
103 subclinical disease management, and risk stratification and reduce disease-associated morbidity
104 and mortality. Already identified potential biomarkers include markers of myocardial injury,
105 cardiac mechanical stretch, inflammation, and hemostasis imbalance; however, with the
106 exception of lipoprotein(a), these are not specific to CAVD or have yet to be validated in large
107 randomized studies (32).

108 The aortic valve develops from rudimentary endocardial cushions that are subsequently
109 refined into thin leaflets well into postnatal life. This process is dependent on complex cell-ECM
110 interactions and is modulated by hemodynamics, and its spatio-temporal dysregulation results in
111 malformations and maladaptive remodeling (10). Several lines of evidence indicate that valve
112 disease at any age is accompanied by some underlying structural defect (29), suggesting that
113 latent CAVD has a developmental origin. Moreover, developmental pathways may also be re-
114 activated during tissue repair processes in the disease setting. For example, molecular
115 mechanisms controlling heart valve cell differentiation are shared with cartilage, tendon, and
116 bone development (reviewed in (15), and are reactivated during endochondral ossification and
117 mature lamellar bone formation taking place in end-stage aortic valve disease (18). Remarkably,
118 only end-stage CAVD has been described at the molecular level, whereas the molecular
119 underpinnings of subclinical disease are poorly understood, due in part to difficulties in
120 accessing biological material from early lesions.

121 To gain mechanistic insight, we performed an RNA-seq analysis of human fetal and adult
122 control and calcified bicuspid (cBAV) and tricuspid valves (cTAV). K-means clustering was
123 used to identify dynamically regulated processes taking place simultaneously at crucial stages of

124 human valve development and in diseased valves. The prevailing gene signatures were
125 associated with immune-metabolic processes and heretofore uncharacterized pathways linked to
126 cellular stress and ageing. A search for genes shared between our gene expression datasets and
127 datasets generated from asymptomatic subjects from the Progression of Early Subclinical
128 Atherosclerosis (PESA) cohort (5) with aortic valve calcification and without AS identified
129 marker genes in peripheral blood of asymptomatic individuals. When combined in quantitative
130 RT-PCR assays, these marker genes showed good sensitivity and specificity for predicting
131 CAVD at a subclinical stage.

132 RESULTS

133 Diseased valves are transcriptionally more similar to developing valves than to controls

134 Genome-wide transcriptome profiling was carried out on normal adult control valves
135 (n=8) and severely stenotic calcified BAV (cBAV; n=5) and TAV (cTAV; n=7) valves, as well
136 as on fetal aortic valves at gestational weeks 9 (n=4), 12-13, (n=3) and 22 (n=2) (Supplementary
137 Table S1, see <https://figshare.com/s/4357d56025cb3380a0df>). These developmental timepoints
138 correspond to mouse embryonic days (E) 13.5-17.5 (13), during which valves are remodeled by
139 morphogenic processes leading to thinning, elongation, and formation of multi-laminar valve
140 structure. To integrate data across studies and generalize our findings, we conducted a meta-
141 analysis with publicly available expression data from normal adult control (n=8), cBAVs (n=10),
142 and cTAVs (n=9) valves (8) (Figure 1A). After correcting for batch effects, Principal Component
143 Analysis (PCA) indicated that sample differences did not correlate with batch origin
144 (Supplementary Fig. S1A), but rather depended on disease or developmental stages (Figure 1B).
145 The first of the PCA components (PC1) separated developing and adult valve samples according
146 to disease severity, ranging from cTAV (right hand side) to controls (left hand side).
147 Interestingly, fetal valves tended to cluster with diseased adult valves. There were two control
148 samples (both from heart transplants) and one sample of embryonic samples at 9 weeks showing
149 more heterogeneity than the rest according to the second component (y-axis) but still the range of
150 the axis (-0.6 to 0.4) is very small, confirming the reproducibility of the samples in terms of
151 global transcriptome. In the second PCA component (PC2), the adult control and disease samples
152 were separated from fetal weeks 9 and 13 samples (Figure 1B). Therefore, and considering that
153 the first PCA dimension explains 15.24% of the variance, while the second dimension explains
154 only 7.73%, adult disease samples appeared to be more closely related to fetal than to control
155 samples, suggesting that some of the disease pathogenesis can be ascribed to the recapitulation of
156 developmental processes.

157 To further support this finding, we used Euclidean distances between overall gene
158 expression profiles to perform hierarchical clustering (HC) of the samples (Figure 1C). Similar
159 to what was observed in the PCA, disease samples cluster further apart from controls and appear
160 under the same branch with embryonic samples at 9 and 13 weeks.

161

162 **Clustering identifies dynamic gene expression across disease and developmental states**

163 Differential expression analysis was initially carried out between each pair of conditions of
164 interest (Supplementary Table S2, see <https://figshare.com/s/4357d56025cb3380a0df>
165 ; 9 pairwise comparisons). However, pair-wise comparisons were not adequate to explore
166 dynamic and coordinated gene expression profiles across different disease and developmental
167 states. K-means analysis computing n=50 yielded dynamic expression profiles across the
168 different conditions (Supplementary Fig. S1B, see
169 <https://figshare.com/s/d9a68e0d6faa67e4c6c3>). Co-expressed genes (ie. genes undergoing
170 similar disease/stage status expression changes) likely participate in the same process, and genes
171 that function in the same process are regulated coordinately (20). There were 6 broad
172 combinations of expression patterns: 1) genes down-regulated in developing valves and up-
173 regulated in control adult valves (e.g. C34); 2) genes down-regulated in control and up-regulated
174 in diseased valves (e.g. C7); 3) genes up-regulated in developing valves, down-regulated in adult
175 control valves, and up-regulated in diseased valves (e.g. C45); 4) genes up-regulated in
176 developing valves and down-regulated in adult control and disease valves (e.g. C37); 5) genes
177 up-regulated in adult control valves and down-regulated in diseased valves (e.g. C16); and 6)
178 genes down-regulated in developing valves, up-regulated in adult control valves, and down-
179 regulated in diseased valves (e.g. C40) (Supplementary Fig. S1B, see
180 <https://figshare.com/s/d9a68e0d6faa67e4c6c3>). Thus, part of the disease process involves a gene
181 signature present during fetal valve development.

182

183 **Comparative functional analysis identifies multiple interconnected pathways**

184 Functional enrichment analysis of clusters with IPA identified significant associations to
185 canonical pathways in 28 clusters (Figure 2). Subsequent unsupervised hierarchical clustering of
186 clusters, based on the fraction of shared canonical pathways, identified 6 metaclusters (MC),
187 termed MC1-MC6 (Figure 2). Cluster 10 did not overlap with the others in terms of functional
188 enrichment, and was not further considered. Generally, genes highly expressed in adult disease
189 showed low expression at gestational week 13 and vice-versa; however, there were exceptions
190 (clusters 9, 12, 23, and 45; Figure 2). Although metaclusters were defined as non-overlapping
191 collections of gene clusters, enriched functions could be shared between several meta-clusters.
192 For example, canonical pathways associated to clusters 46 and 32 were shared by MC1 and
193 MC2; those associated to cluster 12 were shared by MC2, MC3, MC4, and MC6; those to
194 clusters 12 to 45 were shared by MC2, MC3, and MC4; and those canonical pathways enriched
195 in clusters 5 and 45 were shared by MC4 and MC6 (Figure 2). Therefore, the biological
196 functions represented in the different MCs are interconnected.

197

198 **Innate and adaptive immune processes are present in valve disease and development**

199 The collections of genes associated to metaclusters MC1-MC6 were reanalysed with IPA.
200 Enriched canonical pathways associated to each MC are summarized in Figure 3. MC3 was
201 associated to 168 pathways related to innate-adaptive immune processes (Supplementary Fig. S2,
202 see <https://figshare.com/s/d9a68e0d6faa67e4c6c3>). The top 5 pathways were Th1 and Th2
203 Activation Pathway, TREM1 Signaling, Communication between Innate and Adaptive Immune
204 Cells, Phagosome Formation and Dendritic Cell Maturation (Figure 3; Supplementary Fig. S3,
205 see <https://figshare.com/s/d9a68e0d6faa67e4c6c3>; Supplementary Table S3, see
206 <https://figshare.com/s/4357d56025cb3380a0df>). The remaining 163 enriched biological
207 functions were also involved in critical immune-inflammatory cellular processes (Supplementary
208 Fig. S2, see <https://figshare.com/s/d9a68e0d6faa67e4c6c3>; Supplementary Table S3, see

209 <https://figshare.com/s/4357d56025cb3380a0df>). Among the nine clusters combined into MC3,
210 five of them had expression profiles characterised by increased gene expression in all adult
211 samples, both control and CAVD (clusters 22, 9, 34, 36 and 2), whereas four clusters had
212 increased expression in CAVD only (clusters 49, 44, 7, and 35; Figure 3). Discrete immune cell
213 gene signatures were present at week 9 (clusters 44 and 35), week 13 (cluster 9), and week 22
214 (clusters 49 and 22) of development (Figure 3), but involved relatively fewer pathways than
215 those found in control or calcified adult valves. The presence of immune and pro-inflammatory
216 gene signatures during fetal development and in apparently healthy valves is consistent with the
217 progressive nature of the calcified valve disease pathology.

218

219 **Cell migration and DNA replicative pathways are re-activated in CAVD**

220 Metaclusters MC4 and MC6 were enriched in genes belonging to 202 and 23 IPA pathways,
221 respectively (Supplementary Fig. S4 and S6A, see
222 <https://figshare.com/s/d9a68e0d6faa67e4c6c3>; Supplementary Table S3, see
223 <https://figshare.com/s/4357d56025cb3380a0df>). In general, genes associated to these clusters
224 have increased expression during development (notably at week 13), decreased in adulthood and
225 re-activated in CAVD. Therefore, of the 7 clusters associated with these two MCs, six were
226 associated with more elevated gene expression in the diseased state (clusters 25, 23, 5, 45, 17,
227 and 21), whereas only one was associated with lower expression (cluster 40; Figure 3). The top
228 five pathways in MC4 were Actin Cytoskeleton Signaling, Molecular Mechanisms of Cancer,
229 Axonal Guidance Signaling, Epithelial Adherens Junction Signaling and Integrin Signaling
230 (Figure 3, Supplementary Fig. S5, Supplementary Table S3, see
231 <https://figshare.com/s/4357d56025cb3380a0df>). The remaining 197 IPA pathways, represented
232 components of fundamental cell and developmental signaling pathways (Supplementary Fig. S4,
233 see <https://figshare.com/s/d9a68e0d6faa67e4c6c3>; Supplementary Table S3, see
234 <https://figshare.com/s/4357d56025cb3380a0df>). The top five pathways in MC6 were Role of

235 CHK Proteins in Cell Cycle Checkpoint Control, Sumoylation Pathway, Cell Cycle Control of
236 Chromosomal Replication, Cell Cycle: G2/M DNA Damage Checkpoint Regulation, Role of
237 BRCA1 in DNA Damage Response (Figure 3, Supplementary Fig. S6B, see
238 <https://figshare.com/s/d9a68e0d6faa67e4c6c3>, Supplementary Table S3, see
239 <https://figshare.com/s/4357d56025cb3380a0df>). The remaining 18 IPA pathways were involved
240 in similar processes (Supplementary Fig. S6A, see
241 <https://figshare.com/s/d9a68e0d6faa67e4c6c3>; Supplementary Table S3, see
242 <https://figshare.com/s/4357d56025cb3380a0df>). Cellular proliferation and migration may be
243 part of the ongoing immune-inflammatory response associated with processes represented in
244 MC3.

245

246 **Decreased OXPHOS and ribosomal biogenesis in CAVD**

247 Genes in MC2 were significantly associated to 83 IPA pathways (Supplementary Fig. S7, see
248 <https://figshare.com/s/d9a68e0d6faa67e4c6c3>; Supplementary Table S3, see
249 <https://figshare.com/s/4357d56025cb3380a0df>), the top 5 of which were Mitochondrial
250 Dysfunction, EIF2 Signaling, Oxidative Phosphorylation, Sirtuin Signaling Pathway
251 (Supplementary Fig. S8A-C), Regulation of eIF4 and p70S6K Signaling (Supplementary Fig.
252 S8D,E see <https://figshare.com/s/d9a68e0d6faa67e4c6c3>; Supplementary Table S3, see
253 <https://figshare.com/s/4357d56025cb3380a0df>). The remaining 78 pathways in MC2 were also
254 implicated in energy production and protein metabolism (Supplementary Fig. S7, see
255 <https://figshare.com/s/d9a68e0d6faa67e4c6c3>; Supplementary Table S3, see
256 <https://figshare.com/s/4357d56025cb3380a0df>), showing strong enrichment in genes for nuclear
257 encoded subunits of the electron transport chain complexes and ribosomal biogenesis
258 (Supplementary Fig. S8A-C, see <https://figshare.com/s/d9a68e0d6faa67e4c6c3>; Supplementary
259 Table S3, see <https://figshare.com/s/4357d56025cb3380a0df>). Other gene signatures were AMP-
260 activated protein kinase (AMPK), ER stress (Unfolded protein response), oxidative stress

261 response (NRF2-mediated Oxidative Stress Response), cellular longevity (Telomerase
262 Signaling), and neurodegenerative disease (Huntington's Disease Signaling; Supplementary Fig.
263 S7, see <https://figshare.com/s/d9a68e0d6faa67e4c6c3>; Supplementary Table S3, see
264 <https://figshare.com/s/4357d56025cb3380a0df>), suggesting the modulation of cellular stress
265 responses, and age-related disease gene signatures. Of the nine clusters in MC2, six had, on
266 average, decreased expression in disease conditions (clusters 24, 31, 32, 16, 41, and 1), while
267 one had increased expression in the diseased state (cluster 12) and three were unchanged
268 (clusters 31, 26, and 37; Figure 3). In general, MC2 transcripts had peak expression at week 13,
269 with lower expression at the other developmental stages (Figure 3), suggesting that metabolic
270 processes are dynamically regulated during aortic valve development. Overall, this analysis
271 indicates that CAVD is associated with decreased OXPHOS metabolism and altered proteostasis.

272

273 **Stress response gene signatures are altered in CAVD**

274 MC1 and MC5 did not overlap significantly with any of the other MCs but included similar
275 biological processes. Genes in MC1 were associated to 7 pathways (Figure 3; Supplementary
276 Fig. S9A, see <https://figshare.com/s/d9a68e0d6faa67e4c6c3>; Supplementary Table S3, see
277 <https://figshare.com/s/4357d56025cb3380a0df>), the top 5 being Sphingosine-1-phosphate
278 Signaling, Endocannabinoid Developing Neuron Pathway, Amyloid Processing, Huntington's
279 Disease Signaling, Dermatan Sulfate Degradation (Figure 3; Supplementary Fig. S9B, see
280 <https://figshare.com/s/d9a68e0d6faa67e4c6c3>; Supplementary Table S3, see
281 <https://figshare.com/s/4357d56025cb3380a0df>). The expression of MC1 genes was relatively
282 increased in adult controls and decreased in CAVD (Figure 3). MC5 was enriched in a single
283 pathway, Unfolded protein response (Figure 3; Supplementary Fig. S9C, see
284 <https://figshare.com/s/d9a68e0d6faa67e4c6c3>; Supplementary Table S3, see
285 <https://figshare.com/s/4357d56025cb3380a0df>). MC5 genes were expressed at decreased levels
286 in controls and increased in CAVD (Figure 3). These data suggest that chronic immune-

287 inflammatory processes are linked to cellular stress and age-related disease in calcific aortic
288 valve pathology.

289

290

291 **Identification of circulating biomarkers predicting CAVD**

292 To identify potential biomarkers useful for predicting CAVD, a sub-set of genes from the aortic
293 valve study was compared with whole blood RNA-Seq data from asymptomatic individuals with
294 aortic valve calcification, detected by non-contrast computed tomography in the *Progression of*
295 *Early Subclinical Atherosclerosis* (PESA) study (5). PESA participants undergo simultaneous
296 cardiac calcium scoring and blood sampling. Out of the 455 PESA participants for which RNA-
297 seq data was available in visit 2 (ie. three years after recruitment), 59 had evidence of valve
298 calcification and 52 of these had sufficient integrity for qPCR analysis. None of them had
299 valvular stenosis/regurgitation, evidencing an early stage of the disease. Their transcriptome was
300 compared to the transcriptome of PESA individuals without valvular calcification (n=395). From
301 the whole set of genes identified as differentially expressed (p<0.05, Supplementary Table S5,
302 see <https://figshare.com/s/4357d56025cb3380a0df>), six were selected that showed a disease-
303 specific pattern in the RNA-seq data of human aortic valves (see Methods for selection criteria;
304 Supplementary Fig. S1, see <https://figshare.com/s/d9a68e0d6faa67e4c6c3>). Five of these genes
305 were related to adaptive innate and adaptive responses (*CD28, ITK, PAG1, NLRC5, and ASCC3*)
306 and a sixth was related to the WNT pathway (*LINS1*) (Supplementary Table S6, see
307 <https://figshare.com/s/4357d56025cb3380a0df>). The expression of the six genes was measured in
308 whole blood (WB) on 104 PESA participants [52 cases: asymptomatic individuals with
309 calcification of the aortic valve (PESA-SD); 52 controls: individuals without calcification
310 (PESA-CTL)] and 12 patients with CAVD recruited at Montepincipe Hospital (WB-CAVD) by
311 qRT-PCR and correlated with the degree of aortic valve calcification (Figure 4A, Supplementary
312 Table S4, see <https://figshare.com/s/4357d56025cb3380a0df>). Considering all conditions, the 6

313 genes showed some degree of correlation when considered individually ($P \leq 0.27$; Figure 4A,
314 Supplementary Table S7, see <https://figshare.com/s/4357d56025cb3380a0df>). Given that,
315 *NLRC5* and *PAG1* were also associated with total calcification of the coronaries (Supplementary
316 Fig. S10A, see <https://figshare.com/s/d9a68e0d6faa67e4c6c3>, Supplementary Table S7, see
317 <https://figshare.com/s/4357d56025cb3380a0df>) and were therefore excluded as potential specific
318 markers of aortic valve calcification.

319 To determine the utility of *ASCC3*, *ITK*, *CD28* and *LINS1* as potential markers of valve
320 calcification, a ROC curve was built to represent the predictive value of the model to classify
321 calcific disease patients (WB-CAVD) vs PESA-SD individuals and vs PESA-CTL, yielding
322 areas under the curve (AUCs) of 0.97 and 0.91 respectively (Figure 4B). An additional model
323 was built to assess the power of the gene signature to distinguish between individuals without
324 calcification (PESA-CTL) from those with subclinical disease (PESA-SD; AUC=0.71).

325 This model was then validated in whole blood samples of an independent cohort of
326 CAVD patients (n=16), together with samples from 25 of the 52 PESA-SD individuals and 35 of
327 the 52 PESA-CTL individuals taken three years after visit 2 (Figure 4C). The model achieved
328 AUCs of 0.90 and 0.88 to discriminate CAVD patients from PESA-SD and PESA-CTL
329 individuals, respectively. The AUC of the model to distinguish PESA-SD from PESA-CTL was
330 again 0.71 (Figure 4C). Thus, our model identifies a gene expression signature in blood that is
331 highly predictive of valve disease and of aortic valve calcification levels in otherwise healthy
332 individuals.

333

334 **DISCUSSION**

335 This study provides, for the first time, a comprehensive molecular profile of shared and unique
336 cellular activities taking place in aortic valve development and CAVD. The transcriptome of
337 adult disease samples appeared to be more closely related to fetal week 9 than to control samples
338 or weeks 13 and 22, suggesting that some of the disease pathogenesis might be ascribed to the
339 recapitulation of processes taking place in early development. The overall cBAV and cTAV gene
340 expression profiles were essentially identical, confirming previous findings suggesting that valve
341 calcification depends on the same biological pathways, regardless of valve morphology (8, 26).
342 Therefore, the mechanisms leading to BAV formation are independent of those leading to BAV
343 calcification; in other words, the cause of the embryonic defect is distinct from the resulting
344 calcification process.

345 Functional analysis provided compelling evidence that innate and adaptive immune
346 interactions take place in the aortic valve throughout life (Supplementary Fig. S10B 13, see
347 <https://figshare.com/s/d9a68e0d6faa67e4c6c3>). The fetal immune cell gene signature in MC3
348 was notably simpler than in adult control or CAVD samples, with fewer immune cell gene
349 expression signatures present at gestational weeks 9 (3/9 clusters), 13 (1/9 clusters), or 22 (3/9
350 clusters) than in adult controls (5/9 clusters) or in CAVD (9/9 clusters), suggesting that aortic
351 valve immune cell enrichment in the aortic valve increases over time. Moreover, the presence of
352 only one immune cell gene signature at 13 weeks (cluster 9), compared with three at 9 and 22
353 weeks of gestation, implies that the immune landscape is dynamically regulated in developing
354 valves. These observations are consistent with previous findings of multiphasic changes in shear
355 stress-response, cell-ECM interaction and adaptive immunity pathways from week 14 to week 22
356 of human aortic valve development (7).

357 The predominant T cell gene signature in the RNA-seq dataset strengthens the notion that
358 unresolved immune-inflammatory response is a major CAVD component (17). This association
359 is well established, with early immunohistological findings indicating the presence of T

360 lymphocytes in immune infiltrates (23, 24). More recent studies have revealed the existence of T
361 cell infiltration in BAV and TAV calcific disease, consisting of non-specific chemokine driven
362 polyclonal T cell recruitment, and memory-effector CD8+ T cell clonal expansions (34, 35),
363 supporting the interpretation of an antigen-induced immune response. Moreover, this antigen-
364 driven response involved circulating expanded CD8+ and, to a lesser extent, CD4+ T cell clones
365 between circulating blood and valve tissues suggesting a systemic disease (34). The gene
366 expression signatures of several other immune-competent cells, including B-lymphocytes,
367 macrophages, and dendritic cells were also present, confirming previous characterization of
368 cellular infiltrates in CAVD (33). Together with a body of literature suggesting a tight
369 inflammatory cell-valve interstitial cell interaction in CAVD (11, 17), our data are consistent
370 with the notion that unresolved inflammation ultimately drives myo-fibroblast and osteoblast-
371 like differentiation and leads to heterotopic bone formation. Therefore, targeted therapeutic
372 immunosuppression of calcification might be approachable by better characterizing the various
373 infiltrating immune-cell subtypes.

374 Functional analysis revealed that OXPHOS metabolism was decreased in CAVD, with
375 coordinated expression reduction of multiple nuclear genes encoding subunits of mitochondrial
376 electron transport chain complexes I, III, IV and V. These changes might be part of ongoing
377 adaptive metabolic reprogramming during T lymphocyte activation (27), when upon
378 encountering an antigen, T cells proliferate and acquire new functions, switching energy
379 metabolism from OXPHOS to glycolysis. However, both increased and decreased expression of
380 glycolytic pathway components were present, suggesting that decreased OXPHOS metabolism
381 cannot be ascribed solely to T cell activation. Moreover, adult aortic valves showed markedly
382 reduced transcript levels of multiple subunits of the small and large protein ribosomal complexes
383 (RPS and RPL respectively) and eukaryotic translation initiation factors (EIF1-4), possibly
384 reflecting co-ordinate dysregulation of OXPHOS activity and ribosomal biogenesis (19). This
385 occurred in uncalcified adult valves as well (clusters 31, 37, and 12), suggesting declining

386 function with age. In contrast signatures for cell death and apoptosis (for example in MC3) and,
387 energy-demanding cell processes such as proliferation, DNA repair, and cell movement (in MC4
388 and MC6) were increased, possibly reflecting cellular heterogeneity within the calcified valve.

389 Decreased mitochondrial metabolism and protein translation may be a manifestation of
390 altered physiological stress responses that occur during ageing (30), which is also related to the
391 inability to maintain adaptability to stress and re-establish homeostasis in response to
392 environmental perturbations. Thus, multiple stress-response gene signatures were present in
393 MC2 and to a lesser extent in MC1 and MC5 (Supplementary Fig. S10B, see
394 <https://figshare.com/s/d9a68e0d6faa67e4c6c3>). These included SIRT, a highly conserved family
395 of NAD-dependent deacetylases, linking transcriptional regulation to mitochondrial function,
396 stress resistance, metabolism, cell survival and organismal longevity (3) and mTOR (Mammalian
397 target of rapamycin), a nutrient sensing system which regulates protein synthesis, to promote cell
398 growth and proliferation (19). Moreover, deficiency of the unfolded protein response (UPR)
399 pathway, which is activated by misfolding of newly synthesized proteins as part of the ER stress
400 response (9) contributes to inflammation, disease and ageing. Gene signatures including amyloid
401 processing and Huntington's disease signaling were also featured implying shared calcific valve
402 and neurodegenerative disease mechanisms (Supplementary Fig. S10B, see
403 <https://figshare.com/s/d9a68e0d6faa67e4c6c3>). Therefore, chronic inflammation drives
404 metabolic stress and biological ageing in CAVD.

405 Given the phenomenon of cellular trafficking of T cells between the diseased valve
406 tissue, and circulating blood (34), we reasoned that aortic valve and circulating blood from
407 CAVD patients share common genes that would be absent in subclinical individuals. In the
408 PESA study we identified a subpopulation of asymptomatic individuals in this cohort with > 1
409 valve calcification detected by imaging. Therefore, we searched for circulating biomarkers by
410 comparing the CAVD transcriptomes and whole blood from datasets of the subclinical PESA
411 study population, and identified six differentially expressed genes, four of which were found to

412 predict subclinical and overt valve disease. Therefore *ASCC3*, *ITK*, *CD28*, and *LINS* were
413 specific to aortic valve calcification, whereas *PAG1* and *NLRC5* were also associated with
414 coronary artery calcification, suggesting that valve and vascular calcification proceed by shared
415 and separate mechanisms. These mechanisms have yet to be examined, but noteworthy is that
416 five of six genes belong to T cell activation and NF- κ B pathways. This gene signature could be
417 used in combination with high-resolution imaging for the early diagnosis of valve calcification.

418 *Study Limitations.* A limitation of our study is the low sample numbers especially for
419 week 22 samples (n=2). Investigational studies involving human fetal issue are limited by ethical
420 and legal considerations on medical abortion. Nevertheless, our bioinformatics analysis showed
421 that the week 22 samples clustered together and separated well from the other groups by PCA
422 and we are confident of the robustness of the results involving this group. Moreover, differential
423 expression analysis was performed using limma, a statistical method developed ad-hoc for RNA-
424 seq data with low sample size (28).

425

426

427

428

429 **METHODS**

430 **Study population and aortic valve collection.**

431 Fetuses. Aortic valves from human fetuses were obtained from electively- (weeks 9; n=4 and
432 week 12/13; n=3) or medically (week 22; n=2) -terminated pregnancies after written informed
433 consent in concordance with French legislation (PFS14-011) and prior protocol approval from
434 the “Agence de la biomédecine” (Supplementary Table S1, see
435 <https://figshare.com/s/4357d56025cb3380a0df>). Aortic valves were recognized by their
436 anatomical landmarks under the microscope and leaflets were isolated with minimal aortic wall
437 contamination. Samples were immediately flash frozen in liquid nitrogen. The investigation
438 conformed to the principles outlined in the *Declaration of Helsinki*.

439 Patients. The CAVD study population consisted of BAV (n=5) or TAV (n=7) patients referred
440 for aortic valve or aortic root surgery at Montepincipe Hospital and Hospital Clínico San Carlos
441 (Madrid, Spain; Supplementary Table S1, see <https://figshare.com/s/4357d56025cb3380a0df>).
442 Patients were prospectively recruited between December 2009 and February 2013. Patients with
443 a history of rheumatic heart disease, infective endocarditis, or connective tissue disorders were
444 excluded. To determine the morphology and functional state of the aortic valve, all patients
445 underwent clinical evaluation and preoperative 2-dimensional echocardiography according to the
446 *American Heart Association* and the *American College of Cardiology* guidelines (21). The
447 aortic valve morphology and the presence of valvular degeneration, including the extent of
448 leaflet calcification, thickening, prolapse, and/or redundancy, were documented at surgery.
449 Calcification was graded as mild (1/3 leaflet area affected) or severe (2/3 leaflet area affected).
450 Immediately following surgical removal, a portion of the aortic valve leaflet was placed in sterile
451 saline buffer and stored at -80°C until processing. Control valve samples were obtained at
452 autopsy of individuals without cardiac problems who suffered a traumatic death (n=6) or at time
453 of transplantation from heart transplant recipients with normal aortic valves (n=2). All patients or
454 close relatives (for autopsy controls) gave written informed consent, and the study was approved

455 by the Health Service Ethics Committees (Comité Ético de Investigación Clínica) of participant
456 centers. The investigation conformed to the principles outlined in the *Declaration of Helsinki*.

457 Whole-blood samples. Genes of interest were quantified by quantitative reverse transcription-
458 polymerase chain reaction (qRT-PCR) in whole-blood (WB) samples from age-matched case-
459 control males (n=104) of the Progression of Early Subclinical Atherosclerosis (PESA).
460 Subclinical cases (PESA-SD) were defined as participants with aortic-valve calcification score
461 >1, as assessed by the Agatston method (1). Controls (PESA-CTL) had no calcification of the
462 aortic valves or coronary arteries. Patients with aortic valve stenosis and moderate to severe
463 calcification (WB-CAVD; n=12) were recruited from Montepincipe Hospital (Supplementary
464 Table S4, see <https://figshare.com/s/4357d56025cb3380a0df>). For validation, an independent
465 cohort of mainly severe aortic valve stenosis patients (n=16) was obtained from the MRVALVE
466 study. Whole blood was collected in PAXGene tubes (BDBiosciences) and stored at -80°C
467 before processing.

468 **RNA isolation**

469 For each valve, total RNA from a single aortic valve cusp was extracted using the TRIzol LS
470 (Invitrogen, Carlsbad, CA, USA) method and digested with RNase free DNase I (Invitrogen).
471 For PESA and CAVD validation total RNA was using either the PAXgene blood mRNA kit
472 (PreAnalytiX, Hombrechtikon, Switzerland) for manual isolation or the QIASymphony PAXgene
473 blood RNA kit (PreAnalytiX) for automated isolation using a QIASymphony SP liquid handling
474 robot (Qiagen, Venlo, Netherlands). RNA purity, concentration, and integrity were assessed by
475 Nanodrop 2000 spectrophotometry (Thermo Scientific) and automated electrophoresis in a 2100
476 Bioanalyzer (RNA6000 Nano LabChip; Agilent). Samples with a RIN > 6 were selected for
477 reverse transcription.

478 **RNA-seq data generation**

479 RNA-seq was performed on DNase I-treated RNA samples with a RIN > 7. RNA-seq libraries
480 were created using the TruSeq Stranded Total RNA with Ribo-Zero Gold Prep Kit (Fetal

481 samples) or TruSeq™ RNA Sample Prep Kit v2 (Patient samples; Illumina, Diego, CA). Final
482 cDNA libraries were checked for quality and quantified in the 2100 Bioanalyzer (Agilent). The
483 libraries were loaded in the flow cell at 8 pM, and clusters were generated in Cbot and sequenced
484 as 50bp single-end reads on a Hiseq 2500 instrument (adult samples) or 75 base single-end reads
485 on a Genome Analyzer Iix instrument (fetal samples; Illumina, Diego, CA). Image analysis and
486 base calling were performed using RTA and CASAVA.

487 **Bioinformatics analysis of RNA-Seq.**

488 Data preprocessing

489 FASTQ files were pre-processed with cutadapt (16) to eliminate Illumina adapter remains and
490 reads were aligned to the human reference transcriptome (GRCh38.78) using RSEM 1.2.31 (14).
491 Raw data from 27 RNA-seq samples from GSE76718 were downloaded from GEO and pre-
492 processed and aligned using the same pipeline. Control samples were present in all experiments,
493 allowing for batch correction of the data using ComBat (12). Data were normalized using TMM
494 with log-ratio trimming=0.3 and sumTrim=0.05 and voom-transformed. Only genes with at least
495 1 cpm in at least 10 samples were considered for further analysis.

496 Differential Expression Analysis

497 Differential expression between groups was performed using mixed models with eBayes, as
498 implemented in the Bioconductor limma package (28). A gene was classified as differentially
499 expressed if its Benjamini-Hochberg adjusted *P*-value was < 0.05 in any of the contrasts under
500 study (Supplementary Table S2, see <https://figshare.com/s/4357d56025cb3380a0df>).

501 Clustering and functional analyses

502 To identify groups of genes with similar expression profiles across the six conditions under
503 consideration, k-means clustering was performed with the R ComplexHeatmap package on all
504 expressed genes (19,962 genes). The Elbow method was used to estimate the optimal number of
505 clusters, which was set as k=50. The number of genes per cluster was between 215 and 680.
506 Ingenuity Pathway Analysis (IPA, Qiagen) was then used to identify significant associations

507 between canonical pathways and clusters. Twenty-eight clusters, out of the original collection of
508 50, were found to be associated to at least one canonical pathway with Benjamini-Hochberg (B-
509 H) adjusted P -value < 0.05 (Supplementary Table S3, see
510 <https://figshare.com/s/4357d56025cb3380a0df>). Concordance between canonical pathway
511 profiles was then used to identify groups of clusters that could be associated to similar functions.
512 One cluster (cluster 10) did not share any enriched pathway with any other cluster and was not
513 considered further. The remaining 27 clusters were grouped into six meta-clusters, using the
514 fraction of shared pathways as distance measure. Meta-clusters contained from 332 to 3304
515 genes (Figure 2). IPA was used again to re-annotate meta-clusters (Figure 3).

516 **Data availability**

517 Data are deposited in the NCBI GEO database under accession number GSE148219.

518 **qRT-PCR for validation studies in whole blood**

519 *Selection of candidate genes for qRT-PCR.* We used whole blood transcriptomics data generated
520 in the PESA study to identify genes that might potentially serve as predictors of CAVD. The
521 criteria to select these candidate genes were: (i) Genes differentially expressed between
522 individuals with (n=59) and without (n=396) calcification of the aortic valve (p -value ≤ 0.05) but
523 not differentially expressed between individuals with and without calcification in the coronaries
524 (p -value > 0.05 ; Supplementary Table S5, see <https://figshare.com/s/4357d56025cb3380a0df>).
525 (ii) Aortic valve- specific differentially expressed genes with a top 10% correlation between their
526 expression level and the level of calcification of the aortic valves. (iii) Their expression levels in
527 the RNA-seq samples of the aortic valves were either up-regulated in disease v.s. no disease
528 samples or they were upregulated in early embryonic valve samples and in the diseased samples
529 but not in the control samples. From the 10 genes fulfilling the three criteria, 6 were selected
530 based on their presumptive function (Supplementary Table S6, see
531 <https://figshare.com/s/4357d56025cb3380a0df>).

532 qRT-PCR. RNA samples from PESA and CAVD patients (75ng) was reverse transcribed using
533 the High Capacity cDNA Reverse Transcription kit with RNase Inhibitor (ThermoFisher
534 Scientific). Gene expression was quantified by qPCR using TaqMan probes (ThermoFisher
535 Scientific; Supplementary Table S8) in 52 case-control pairs from the PESA study (case: positive
536 calcification of the aortic valve) and in 12 CAVD patients from Montepincipe Hospital. Each
537 reaction was performed in triplicate and the final reaction volume was set to 10 μ l. qPCRs were
538 conducted in 384-well plates (Cat. no. 4344345; Applied Biosystems) using an ABI PRISM
539 7900HT Sequence Detection System (Applied Biosystems). Each well included 3 μ l (2.25 ng)
540 cDNA, 5 μ l 2x TaqMan Universal Mater Mix (ThermoFisher Scientific), 0.5 μ l 20x TaqMan
541 assay (ThermoFisher Scientific), and 1.5 μ l H₂O. The cycling protocol was 10 min at 95°C
542 followed by 60 cycles of 15 s at 95°C and 60 s at 60°C. Baseline and threshold were set
543 automatically in SD S 2.3 (ThermoFisher Scientific) to calculate Cq values. The Cq values were
544 then imported into qBasePlus (Biogazelle, Zwijnaarde, Belgium) to calculate relative quantities
545 normalised to *GAPDH*. Data were scaled per sample to eliminate potential biases.

546 **Statistical analysis**

547 A linear mixed model was used to assess correlation between the expression of each gene in WB
548 and the degree of calcification in the aortic valve for each disease group (PESA-SD, WB-
549 CAVD) separately. Visualization was performed using the multiplot function and the ggplot2 R
550 package. All samples were jointly analyzed using a linear mixed model with the origin of the
551 samples as random effect. The same analysis was performed to assess the correlation of the gene
552 expression with calcification of the coronaries. Four genes which showed no correlation with the
553 amount of calcium in the coronaries were selected to build a gene expression signature using a
554 multinomial model with interaction for the prediction of the three groups of individuals with
555 different disease severity WB-CAVD>PESA-SD>PESA-CTL. To quantify the predictive power

556 of the gene signature between different groups of individuals a logistic regression model was fit
557 to the data and the corresponding ROC curves were built using the ROCR R package.

558

559

560 **Acknowledgments**

561

562 We thank S. Bartlett for English editing. This work was supported by the Ministerio de Ciencia,
563 Innovación y Universidades from Spain, (grants SAF2016-78370-R, CB16/11/00399, CIBER
564 CV, and RD16/0011/0021, TERCEL) and the Fundación BBVA (grant BIO14_298) and
565 Fundación La Marató TV3 (grant 20153431) to J.L.dIP; and the Fondation pour la Recherche
566 Médicale, grant from l'Institut National de la Santé et de la Recherche Médicale (grant
567 DPC20111123002) and l'Association Française contre les Myopathies (grant TRIM-RD) to
568 S.Z. The cost of this publication was supported in part with funds from the ERDF. The CNIC is
569 supported by the Ministerio de Ciencia, Innovación y Universidades (MCNU), the Instituto de
570 Salud Carlos III (ISCIII), and the Pro CNIC Foundation, and is a Severo Ochoa Center of
571 Excellence (grant SEV-2015-0505).

572 **Author contributions**

573 Donal MacGrogan, PhD: Design of work: Substantial; interpretation of data: Substantial;
574 Writing: original draft: Lead; Writing: review & editing: Lead. final approval of the version to be
575 published.

576 Beatriz Martínez Poveda, PhD: Investigation: Lead; Methodology: Substantial; final approval of
577 the version to be published.

578 Jean-Pierre Desvignes, MD: Investigation: Supporting; final approval of the version to be
579 published.

580 Leticia Fernandez-Friera, MD, PhD: Data curation: Substantial; Formal analysis: Substantial;
581 Investigation: Supporting; final approval of the version to be published.

582 Manuel José Gomez, PhD: Formal analysis: Substantial; Visualization: Substantial; final
583 approval of the version to be published.

584 Eduardo Gil Vilariño, BSc: Investigation: Supporting; final approval of the version to be
585 published.

586 Sergio Callejas Alejano, BSc: Investigation: Supporting; final approval of the version to be
587 published.

588 Pablo Garcia-Pavia, MD, PhD: Investigation: Supporting; final approval of the version to be
589 published.

590 Jorge Solis, MD, PhD: Investigation: Supporting; final approval of the version to be published.

591 Joaquín Lucena, MD, PhD: Investigation: Supporting; final approval of the version to be
592 published.

593 David Salgado, PhD: Data curation: supporting; Formal analysis: supporting; Investigation:
594 supporting; final approval of the version to be published.

595 Gwenaelle Collod-Bérout, PhD: Formal analysis: Supporting; Investigation: Supporting; final
596 approval of the version to be published.

597 Emilie Faure, PhD: Formal analysis: Supporting; Investigation: Supporting; final approval of the
598 version to be published.

599 Alexis Théron, MD: Investigation: Supporting; final approval of the version to be published.

600 Julia Torrents, MD: Investigation: Supporting; final approval of the version to be published.

601 Jean-François Avierinos, MD: Investigation: Supporting; final approval of the version to be
602 published.

603 Lorena Montes, MD: Investigation: Supporting; final approval of the version to be published.

604 Ana Dopazo, PhD: Investigation: Supporting; Supervision: Supporting; final approval of the
605 version to be published.

606 Valentín Fuster, MD, PhD: Investigation: Supporting; Resources: Supporting; final approval of
607 the version to be published.

608 Borja Ibañez, MD, PhD: Investigation: Supporting; Writing – review & editing: Supporting;
609 final approval of the version to be published.

610 Fátima Sánchez-Cabo, PhD: Formal analysis: Equal; Writing – review & editing: Supporting;
611 final approval of the version to be published.

612 Stephane Zaffran, PhD: Investigation: Supporting; Supervision: Supporting; Writing –review &
613 editing: Supporting; final approval of the version to be published.

614 José Luis de la Pompa, PhD: Conceptualization: Lead; Funding acquisition: Lead; Project
615 administration: Lead; Resources: Lead; Supervision: Equal; Visualization: Equal; Writing –
616 review & editing: Supporting.

617

618 **Competing interests**

619 The authors declare no competing interests.

620

621

622

623 **REFERENCES**

- 624 1. **Agatston AS, Janowitz WR, Hildner FJ, Zusmer NR, Viamonte M, Jr., and Detrano**
625 **R.** Quantification of coronary artery calcium using ultrafast computed tomography. *J Am Coll*
626 *Cardiol* 15: 827-832, 1990.
- 627 2. **Beppu S, Suzuki S, Matsuda H, Ohmori F, Nagata S, and Miyatake K.** Rapidity of
628 progression of aortic stenosis in patients with congenital bicuspid aortic valves. *Am J Cardiol* 71:
629 322-327, 1993.
- 630 3. **Chang HC, and Guarente L.** SIRT1 and other sirtuins in metabolism. *Trends*
631 *Endocrinol Metab* 25: 138-145, 2014.
- 632 4. **Coffey S, Cairns BJ, and Iung B.** The modern epidemiology of heart valve disease.
633 *Heart* 102: 75-85, 2016.
- 634 5. **Fernandez-Ortiz A, Jimenez-Borreguero LJ, Penalvo JL, Ordovas JM, Mocoroa A,**
635 **Fernandez-Friera L, Laclaustra M, Garcia L, Molina J, Mendiguren JM, Lopez-Melgar B,**
636 **de Vega VM, Alonso-Farto JC, Guallar E, Sillesen H, Rudd JH, Fayad ZA, Ibanez B, Sanz**
637 **G, and Fuster V.** The Progression and Early detection of Subclinical Atherosclerosis (PESA)
638 study: rationale and design. *Am Heart J* 166: 990-998, 2013.
- 639 6. **Freeman RV, and Otto CM.** Spectrum of calcific aortic valve disease: pathogenesis,
640 disease progression, and treatment strategies. *Circulation* 111: 3316-3326, 2005.
- 641 7. **Gottlieb Sen D, Halu A, Razzaque A, Gorham JM, Hartnett J, Seidman JG, Aikawa**
642 **E, and Seidman CE.** The Transcriptional Signature of Growth in Human Fetal Aortic Valve
643 Development. *Ann Thorac Surg* 106: 1834-1840, 2018.
- 644 8. **Guauque-Olarte S, Droit A, Tremblay-Marchand J, Gaudreault N, Kalavrouziotis**
645 **D, Dagenais F, Seidman JG, Body SC, Pibarot P, Mathieu P, and Bosse Y.** RNA expression
646 profile of calcified bicuspid, tricuspid, and normal human aortic valves by RNA sequencing.
647 *Physiol Genomics* 48: 749-761, 2016.
- 648 9. **Hetz C.** The unfolded protein response: controlling cell fate decisions under ER stress
649 and beyond. *Nat Rev Mol Cell Biol* 13: 89-102, 2012.
- 650 10. **Hinton RB, and Yutzey KE.** Heart valve structure and function in development and
651 disease. *Annu Rev Physiol* 73: 29-46, 2011.
- 652 11. **Hulin A, Hego A, Lancellotti P, and Oury C.** Advances in Pathophysiology of Calcific
653 Aortic Valve Disease Propose Novel Molecular Therapeutic Targets. *Front Cardiovasc Med* 5:
654 21, 2018.
- 655 12. **Johnson WE, Li C, and Rabinovic A.** Adjusting batch effects in microarray expression
656 data using empirical Bayes methods. *Biostatistics* 8: 118-127, 2007.
- 657 13. **Krishnan A, Samtani R, Dhanantwari P, Lee E, Yamada S, Shiota K, Donofrio MT,**
658 **Leatherbury L, and Lo CW.** A detailed comparison of mouse and human cardiac development.
659 *Pediatr Res* 76: 500-507, 2014.
- 660 14. **Li B, and Dewey CN.** RSEM: accurate transcript quantification from RNA-Seq data
661 with or without a reference genome. *BMC bioinformatics* 12: 323, 2011.
- 662 15. **Lincoln J, Lange AW, and Yutzey KE.** Hearts and bones: shared regulatory
663 mechanisms in heart valve, cartilage, tendon, and bone development. *Dev Biol* 294: 292-302,
664 2006.
- 665 16. **Martin M.** CUTADAPT removes adapter sequences from high-throughput sequencing
666 reads. *EMBnetjournal* 17: 10-12, 2011.
- 667 17. **Mathieu P, Bouchareb R, and Boulanger MC.** Innate and Adaptive Immunity in
668 Calcific Aortic Valve Disease. *J Immunol Res* 2015: 851945, 2015.
- 669 18. **Mohler ER, 3rd, Gannon F, Reynolds C, Zimmerman R, Keane MG, and Kaplan**
670 **FS.** Bone formation and inflammation in cardiac valves. *Circulation* 103: 1522-1528, 2001.

- 671 19. **Morita M, Gravel SP, Hulea L, Larsson O, Pollak M, St-Pierre J, and Topisirovic I.**
672 mTOR coordinates protein synthesis, mitochondrial activity and proliferation. *Cell Cycle* 14:
673 473-480, 2015.
- 674 20. **Niehrs C, and Pollet N.** Synexpression groups in eukaryotes. *Nature* 402: 483-487,
675 1999.
- 676 21. **Nishimura RA, Otto CM, Bonow RO, Carabello BA, Erwin JP, 3rd, Guyton RA,
677 O'Gara PT, Ruiz CE, Skubas NJ, Sorajja P, Sundt TM, 3rd, Thomas JD, Anderson JL,
678 Halperin JL, Albert NM, Bozkurt B, Brindis RG, Creager MA, Curtis LH, DeMets D,
679 Guyton RA, Hochman JS, Kovacs RJ, Ohman EM, Pressler SJ, Sellke FW, Shen WK,
680 Stevenson WG, Yancy CW, American College of C, American College of
681 Cardiology/American Heart A, and American Heart A.** 2014 AHA/ACC guideline for the
682 management of patients with valvular heart disease: a report of the American College of
683 Cardiology/American Heart Association Task Force on Practice Guidelines. *J Thorac
684 Cardiovasc Surg* 148: e1-e132, 2014.
- 685 22. **O'Brien KD.** Pathogenesis of calcific aortic valve disease: a disease process comes of
686 age (and a good deal more). *Arterioscler Thromb Vasc Biol* 26: 1721-1728, 2006.
- 687 23. **Olsson M, Dalsgaard CJ, Haegerstrand A, Rosenqvist M, Ryden L, and Nilsson J.**
688 Accumulation of T lymphocytes and expression of interleukin-2 receptors in nonrheumatic
689 stenotic aortic valves. *J Am Coll Cardiol* 23: 1162-1170, 1994.
- 690 24. **Otto CM, Kuusisto J, Reichenbach DD, Gown AM, and O'Brien KD.**
691 Characterization of the early lesion of 'degenerative' valvular aortic stenosis. Histological and
692 immunohistochemical studies. *Circulation* 90: 844-853, 1994.
- 693 25. **Otto CM, and Prendergast B.** Aortic-valve stenosis--from patients at risk to severe
694 valve obstruction. *N Engl J Med* 371: 744-756, 2014.
- 695 26. **Padang R, Bagnall RD, Tsoutsman T, Bannon PG, and Semsarian C.** Comparative
696 transcriptome profiling in human bicuspid aortic valve disease using RNA sequencing. *Physiol
697 Genomics* 47: 75-87, 2015.
- 698 27. **Pearce EL.** Metabolism in T cell activation and differentiation. *Curr Opin Immunol* 22:
699 314-320, 2010.
- 700 28. **Ritchie ME, Phipson B, Wu D, Hu Y, Law CW, Shi W, and Smyth GK.** limma
701 powers differential expression analyses for RNA-sequencing and microarray studies. *Nucleic
702 acids research* 43: e47, 2015.
- 703 29. **Roberts WC, and Ko JM.** Frequency by decades of unicuspid, bicuspid, and tricuspid
704 aortic valves in adults having isolated aortic valve replacement for aortic stenosis, with or
705 without associated aortic regurgitation. *Circulation* 111: 920-925, 2005.
- 706 30. **Schlotter F, Halu A, Goto S, Blaser MC, Body SC, Lee LH, Higashi H, DeLaughter
707 DM, Hutcheson JD, Vyas P, Pham T, Rogers MA, Sharma A, Seidman CE, Loscalzo J,
708 Seidman JG, Aikawa M, Singh SA, and Aikawa E.** Spatiotemporal Multi-Omics Mapping
709 Generates a Molecular Atlas of the Aortic Valve and Reveals Networks Driving Disease.
710 *Circulation* 138: 377-393, 2018.
- 711 31. **Siu SC, and Silversides CK.** Bicuspid aortic valve disease. *J Am Coll Cardiol* 55: 2789-
712 2800, 2010.
- 713 32. **Small A, Kiss D, Giri J, Anwaruddin S, Siddiqi H, Guerraty M, Chirinos JA,
714 Ferrari G, and Rader DJ.** Biomarkers of Calcific Aortic Valve Disease. *Arterioscler Thromb
715 Vasc Biol* 37: 623-632, 2017.
- 716 33. **Steiner I, Krbal L, Rozkos T, Harrer J, and Laco J.** Calcific aortic valve stenosis:
717 Immunohistochemical analysis of inflammatory infiltrate. *Pathol Res Pract* 208: 231-234, 2012.
- 718 34. **Winchester R, Wiesendanger M, O'Brien W, Zhang HZ, Maurer MS, Gillam LD,
719 Schwartz A, Marboe C, and Stewart AS.** Circulating activated and effector memory T cells are
720 associated with calcification and clonal expansions in bicuspid and tricuspid valves of calcific
721 aortic stenosis. *J Immunol* 187: 1006-1014, 2011.

- 722 35. **Wu HD, Maurer MS, Friedman RA, Marboe CC, Ruiz-Vazquez EM,**
723 **Ramakrishnan R, Schwartz A, Tilson MD, Stewart AS, and Winchester R.** The lymphocytic
724 infiltration in calcific aortic stenosis predominantly consists of clonally expanded T cells. *J*
725 *Immunol* 178: 5329-5339, 2007.
- 726 36. **Zhao Y, Nicoll R, He YH, and Henein MY.** The effect of statins on valve function and
727 calcification in aortic stenosis: A meta-analysis. *Atherosclerosis* 246: 318-324, 2016.
728

729 **FIGURE LEGENDS**

730

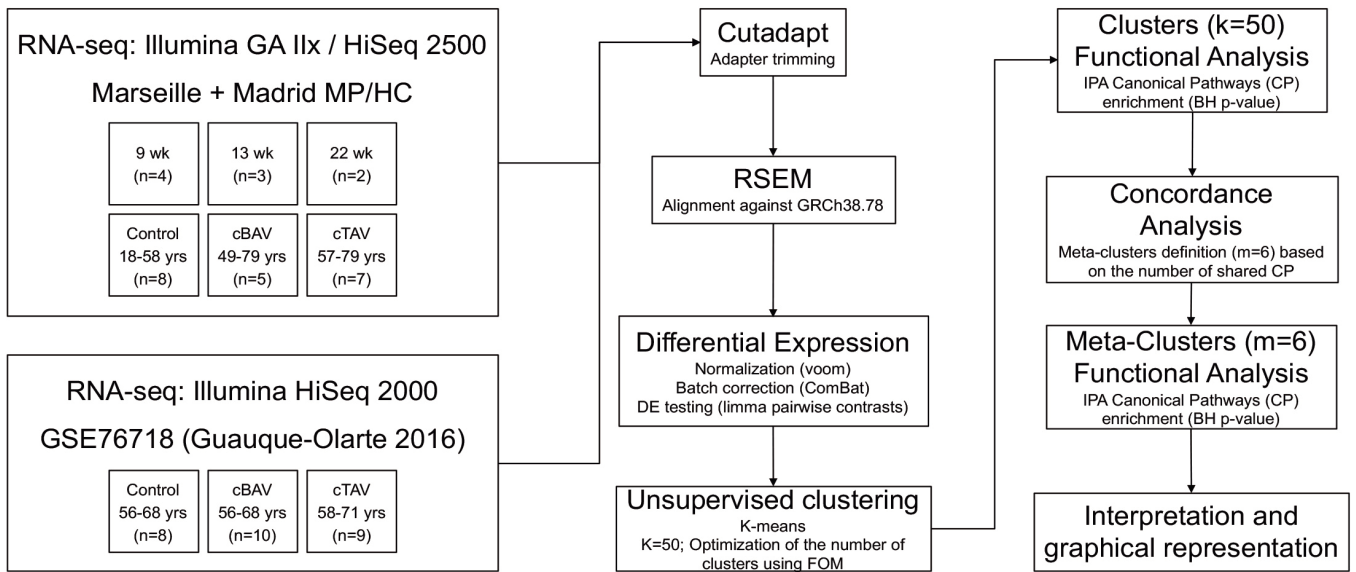
731 **Figure 1.** Aortic valve collection summary, bioinformatics pipeline and mapping of sample
732 batches and biological conditions in gene expression profile-based principal component analysis
733 (PCA) plots. (A) Study outline summarizing aortic valve collection. During the study period,
734 aortic valve leaflets were collected from human fetuses at gestational week (week) 9 (n=4), 12-
735 13 (n=3), and 22 (n=2), adult controls (n=8) and patients with calcified BAV (cBAV; n=5) or
736 TAV (cTAV; n=7). Samples were processed and subject to RNA-seq to characterize their gene
737 expression profiles. Complementary expression data from control, cBAV and cTAV samples
738 was downloaded from GEO (GSE76718). The resulting data set collection was analyzed with a
739 bioinformatics pipeline that included preprocessing of fastq files with cutadapt, alignment
740 against a human transcriptome reference and estimation of gene expression levels with RSEM,
741 and differential expression testing with limma, considering that samples could be ascribed to five
742 experimental batches. Expression profiles were clustered using k-means to obtain a collection of
743 50 clusters, which were then annotated with the Canonical Pathway feature of IPA. Twenty-
744 seven clusters associated to at least one canonical pathway (with Benjamini-Hochberg adjusted
745 p-value < 0.05) were grouped into six meta-clusters on the basis of concordant annotations.
746 Meta-clusters were finally re-annotated with IPA. (B) Hierarchical clustering of the samples
747 overall gene expression based on Euclidean Distance (C) Gene expression profile PCA plot
748 mapping of biological conditions. Sample points are colored according to fetal developmental
749 stage or adult disease state (no disease, n=16; cBAV, n=15 and cTAV, n=16). In PC1, control
750 samples separate from fetal samples and cBAV or cTAV samples. In PC2, early-stage fetal
751 samples (weeks 9 and 13) separate from adult control and disease samples. Percentages on axis
752 labels denote the amount of variance explained by each principal component.
753

754 **Figure 2.** Concordance analysis of k-means clustering. K-means-based gene clusters (see
755 Supplementary Fig. S 1B, see <https://figshare.com/s/d9a68e0d6faa67e4c6c3>) were grouped into
756 metaclusters according to the agreement of their enriched canonical pathways. The white to
757 violet squares in the central heatmap represent the percentage (from 0 to 100) of Canonical
758 Pathways (CP) shared between each pair of 50 k-means clusters for which at least one enriched
759 and shared term was found (k=27 out of the original 50 clusters). Hierarchical clustering of the
760 concordance matrix identified six meta-clusters (MC1-6) The heatmap on the left represents the
761 mean gene expression values for each cluster across biological conditions, on a normalized scale
762 (from -2 to 2, for values below and above the mean, respectively). The dendrogram at the top
763 represents functional relatedness between clusters, which was used to group them into meta-
764 clusters. Meta-clusters are identified with colored boxes (MC1 to MC6, in red, blue, green,
765 purple, orange and yellow, respectively) and represent groups of clusters associated to similar
766 functions.
767

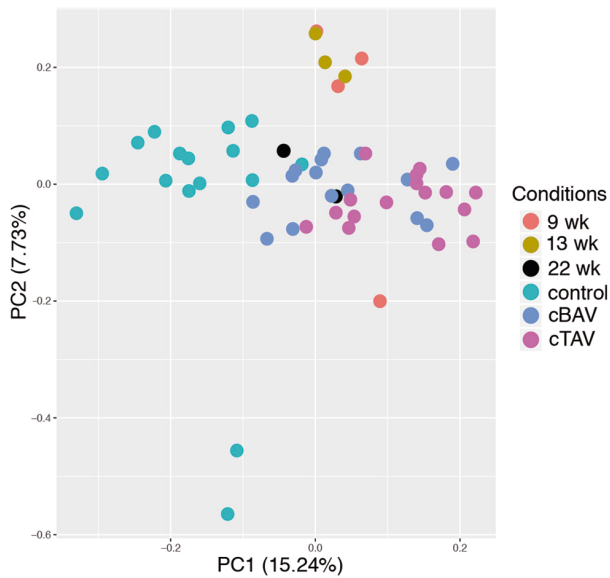
768 **Figure 3.** Functional analysis of meta-clusters. The six gene metaclusters (MC1-6) described in
769 Figure 2 were annotated with IPA. Barplots on the right-hand side represent enrichment values
770 for the top five IPA Canonical Pathways associated with each meta-cluster (MC), selected
771 according to enrichment significance and having an adjusted Benjamini-Hochberg $P < 0.05$. Meta-
772 clusters are identified with colored boxes (MC1 to MC6, in red, blue, green, purple, orange and
773 yellow, respectively) and represent groups of clusters associated to similar functions. Central
774 boxes list all the genes associated with the selection of pathways associated with each
775 metacluster. The heatmap on the left represents normalized expression values for individual
776 genes across biological conditions, on a normalized scale (from -2 to 2, for values below and
777 above the mean, respectively).
778

779 **Figure 4.** A gene expression signature predictive of CAVD. (A) Correlation of qPCR data (y-
780 axis) vs aortic-valve calcification levels (x-axis) for the 6 selected genes in whole blood (WB).
781 Each point represents an individual's level of gene expression (y-axis) and its aortic valve
782 calcification (x-axis). Dots are colored based on the group to which the individual belongs:
783 PESA-CTL (n=52), PESA-SD (n=52) or WB-CAVD (n=12). Solid lines represent the linear
784 model fit for PESA-SD and WB-CAVD patients. Shaded regions represent the confidence of the
785 linear regression estimate for each calcium level. (B) Receiver operating characteristic (ROC)
786 curve of multivariate logistic regression model predicting CAVD (WB-CAVD) vs preclinical
787 aortic-valve calcification (PESA-SD; thick discontinuous line, AUC=0.97) vs valve calcification
788 (PESA-CTL; thick solid line, AUC=0.91). A third ROC curve for the prediction of valve
789 calcification (PESA-SD) vs no calcification (PESA-CTL; thin solid line, AUC=0.71) is shown.
790 The discontinuous diagonal line indicates a fifty-fifty percent chance to predict each group. (C)
791 Follow-up of the model in PESA subgroups after 3 years. Validation in an independent group of
792 CAVD patients (WB-CAVD, n=16) vs a PESA-SD subgroup (n=25; thick discontinuous line,
793 AUC=0.90) vs a PESA-CTL subgroup (n=35; thick solid line, AUC=0.88). A third ROC curve
794 for the prediction of PESA-SD (n=25) vs PESA-CTL (n=35; thin solid line, AUC=0.71) is
795 shown. The thin discontinuous diagonal line indicates a fifty-fifty percent chance to predict each
796 group.
797
798
799

A



B



C

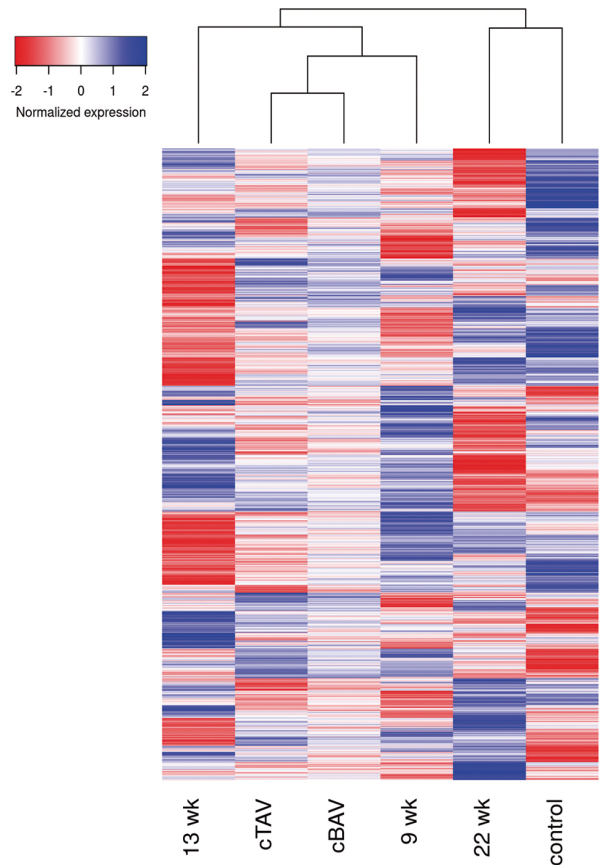


Figure_1_MacGrogan_et_al

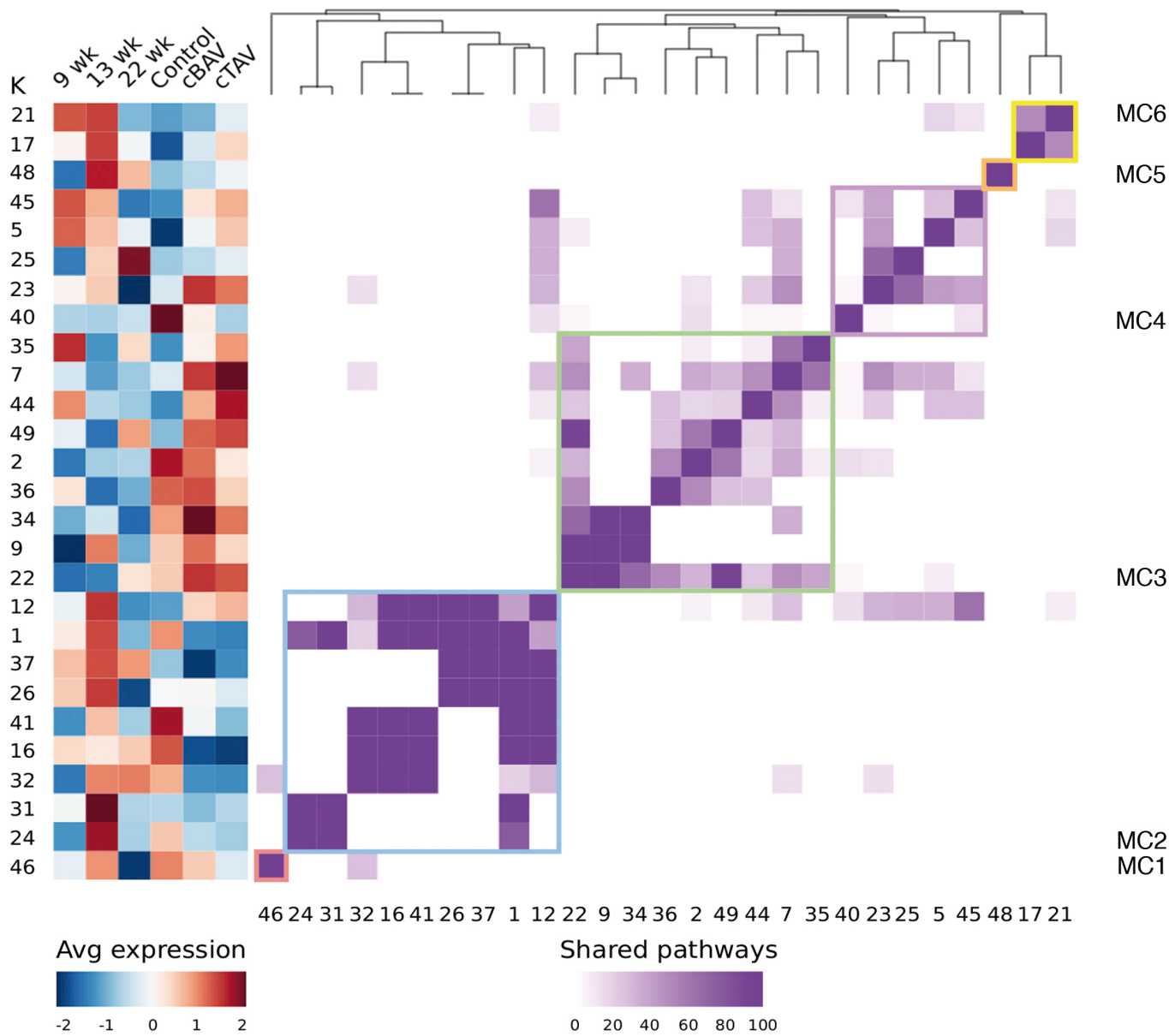
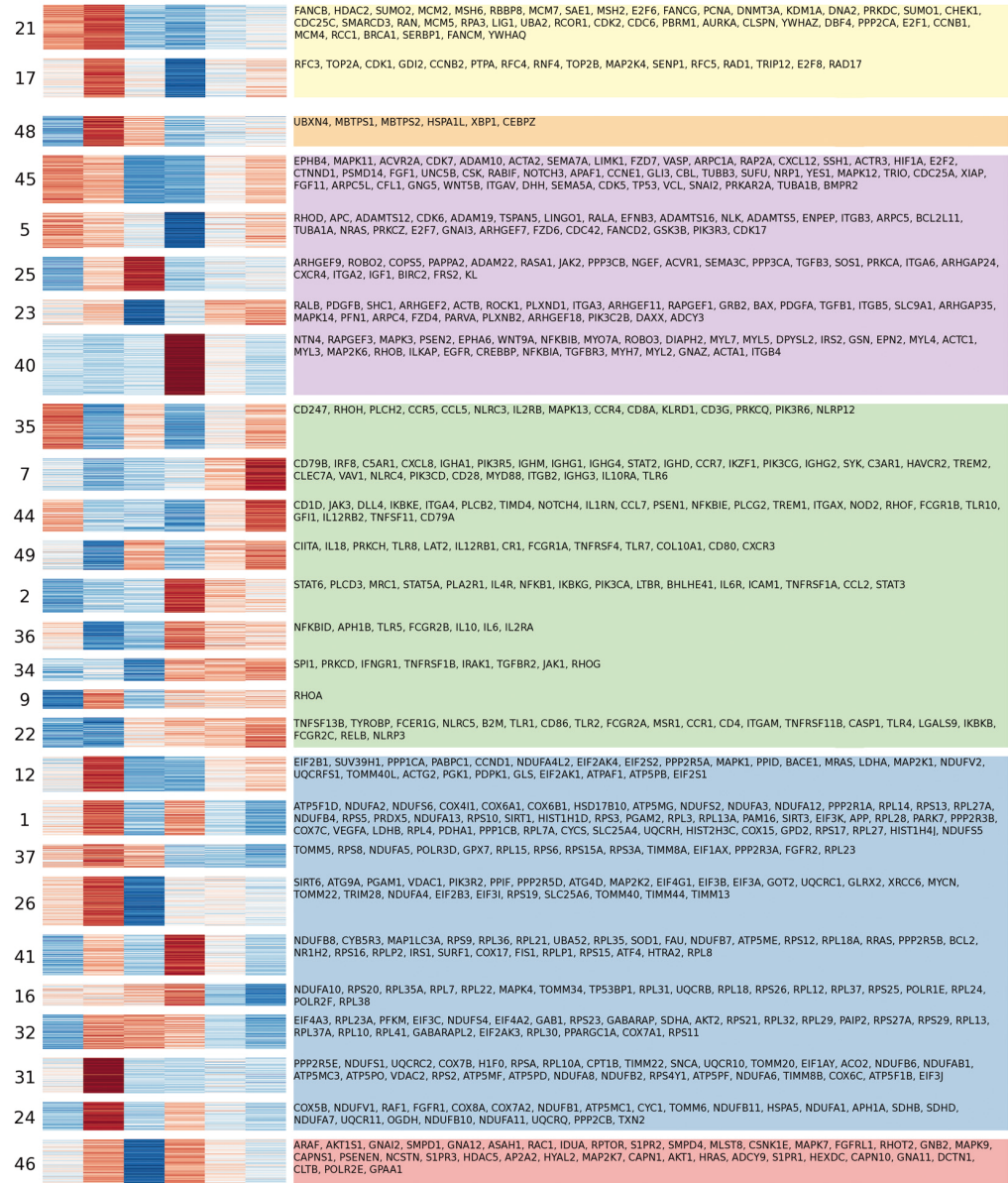


Figure_2_MacGrogan_et_al

K 9 wk
13 wk
22 wk
Control
cBAV
CTAV

Genes in top 5 significant pathways



MC Top 5 significant pathways

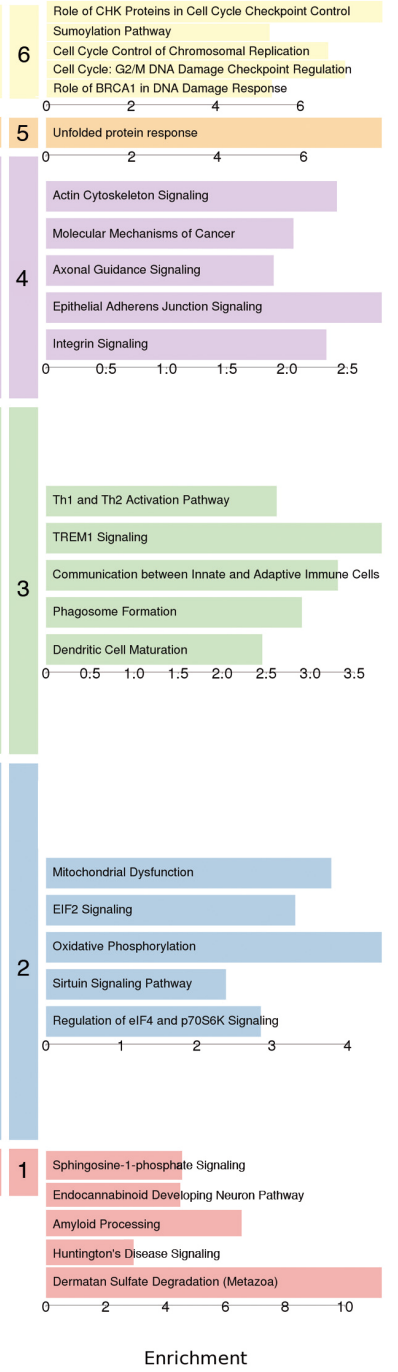
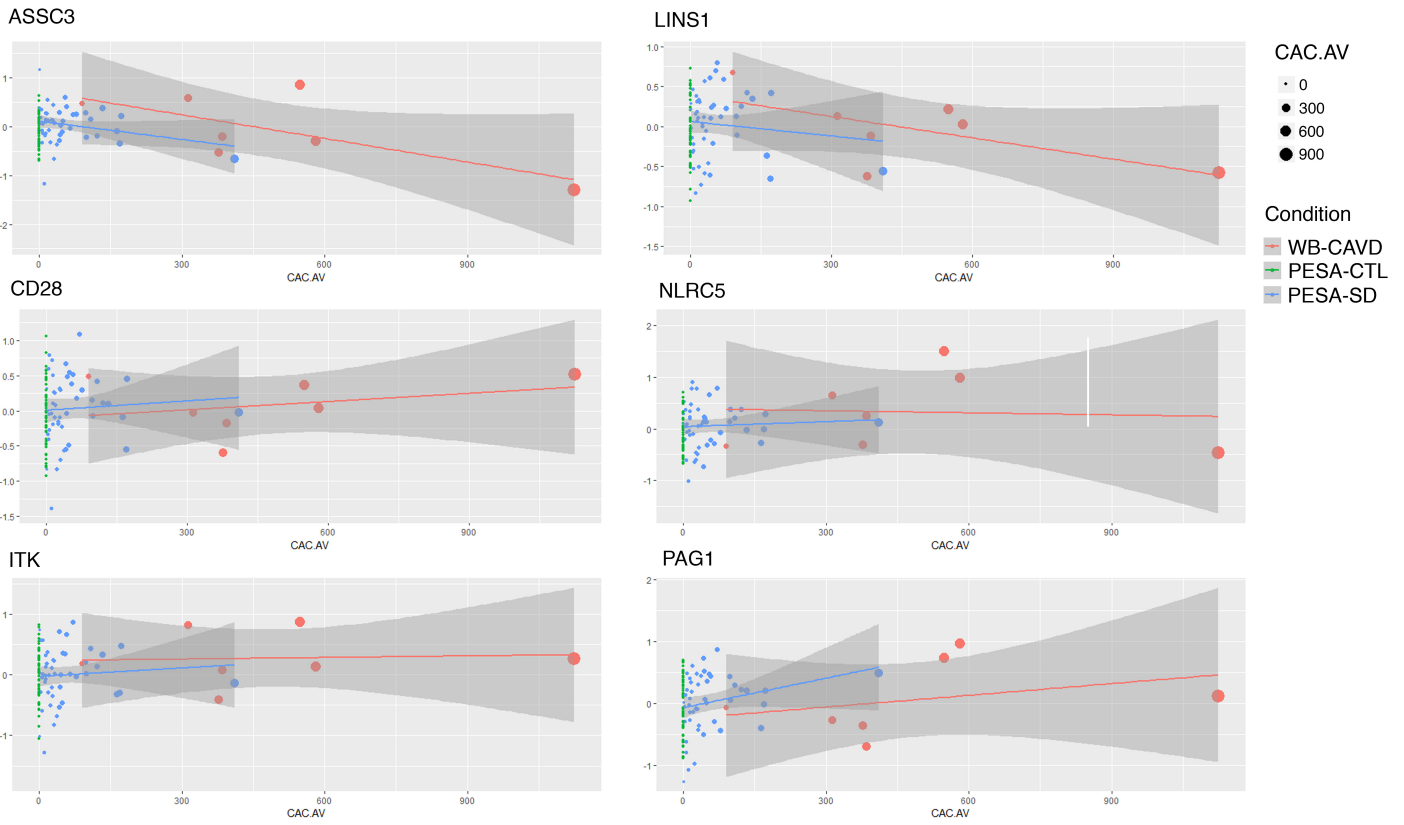
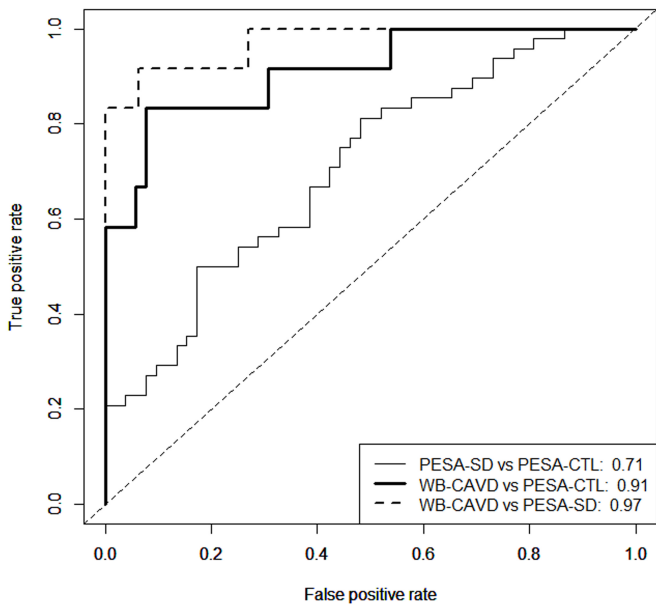


Figure_3_MacGrogan_et_al

A



B



C

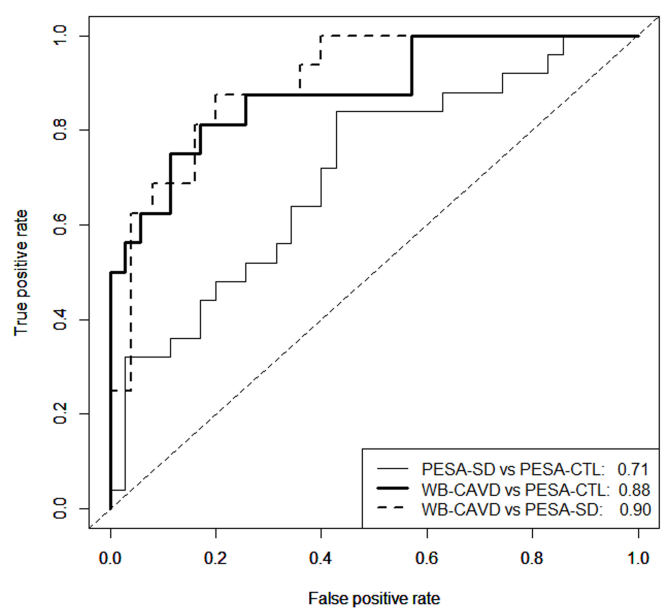


Figure 4_MacGrogan et al